JGR Atmospheres

RESEARCH ARTICLE
10.1029/2025JD044438

The Response of the QBO to External Forcings: Implications for Disruption Events

Chaim I. Garfinkel[1], David Avisar[1,2], Scott Osprey[3], and Doug Smith[4]

[1]Fredy and Nadine Herrmann Institute of Earth Sciences, Hebrew University, Jerusalem, Israel, [2]Department of Applied Math, Environmental Sciences Division, Israel Institute for Biological Research, Ness-Ziona, Israel, [3]Department of Physics, University of Oxford, Oxford, England, [4]Met Office Hadley Centre, Exeter, UK

Key Points:

- ~65,000 years of model output are used to explore the response of the Quasi-Biennial Oscillation (QBO) to external forcings from 1850 to 2020
- Rising greenhouse gas concentrations lead to a weaker QBO with more disruptions, while more aerosols have opposite effect
- Volcanic eruptions prolong QBO westerlies and weaken (even disrupt) the QBO, while ozone invigorates and synchronizes the QBO

Supporting Information:

Supporting Information may be found in the online version of this article.

Correspondence to:

C. I. Garfinkel,
chaim.garfinkel@mail.huji.ac.il

Citation:

Garfinkel, C. I., Avisar, D., Osprey, S., & Smith, D. (2025). The response of the QBO to external forcings: Implications for disruption events. *Journal of Geophysical Research: Atmospheres*, *130*, e2025JD044438. https://doi.org/10.1029/2025JD044438

Received 25 MAY 2025
Accepted 1 NOV 2025

Abstract The response of the Quasi-Biennial Oscillation to changing concentrations of anthropogenic greenhouse gases, aerosols, and ozone, and also to volcanic eruptions and solar variability, is explored using ~65,000 years of model output contributed by four modeling centers to the Large Ensemble Single Forcing Model Intercomparison Project (LESFMIP). The large ensemble size (at least 10, and in many cases 50) allows for the isolation of weak signals that are usually hidden by internal variability. Increasing greenhouse gas concentrations lead to weakening of the Quasi-biennial Oscillation (QBO) and an increased likelihood of a disruption event, with the effect most pronounced in the lower stratosphere. Increasing aerosols lead to a strengthening of the QBO. Explosive volcanic eruptions lead to a weakening, and for some phases also a stalling, of the QBO. Volcanic eruptions can also help trigger a QBO disruption. The ozone forcing used for LESFMIP helps synchronize the QBO phase across ensemble members, and also increases the strength of the QBO. Finally, the solar forcing has the smallest impact on the QBO of the five forcings. The large ensemble sizes also allow for exploring the QBO phases and the time of year most prone to a QBO disruption: disruptions preferentially occur around 8 months after the phase with easterlies near 50 hPa, and are most common in late boreal winter and early spring.

Plain Language Summary The Quasi-biennial Oscillation (QBO) dominates the variability of the tropical atmosphere between 16 and 50 km above the surface. It manifests most strongly as downward propagating zonal wind variations exceeding 25 m/s with an average period of ~28 months. Twice in the past 10 years the QBO regular phase evolution has been disrupted after 60 years of no disruptions, motivating our analysis of the role of greenhouse gases, aerosols, ozone, volcanic eruptions, and solar variability for historical changes in the QBO. We find prominent roles for four of these five external forcings, and specifically both rising greenhouse gases and volcanic eruptions help induce disruption events.

1. Introduction

The Quasi-Biennial Oscillation (QBO) is among the most distinctive internal modes of natural variability in the Earth's climate system. It manifests most clearly as alternate layers of easterly and westerly winds that descend through the equatorial stratosphere from roughly 50 km down to ~16 km (Anstey et al., 2022; Baldwin et al., 2001). Its period ranges from 21 to 32 months, averaging around 28 months, and the oscillation is centered at the equator with a meridional half width of about 12° (Baldwin et al., 2001). The amplitude of the QBO winds peaks at around 30 m/s in the mid-stratosphere. Surface climate is influenced by the QBO through a variety of mechanisms (Garfinkel et al., 2012; Gray et al., 2018; Holton & Tan, 1980; Martin et al., 2021; Rao et al., 2020a, 2020b), and hence it is important to understand how the QBO has changed and will change in the future.

Recent multi-model assessments of changes in QBO amplitude using models contributing to Phase 6 of the Coupled Model Intercomparison Project (CMIP6) have shown that the QBO is expected to weaken in the coming decades, and the weakening is most pronounced in the lower stratosphere (Butchart et al., 2020; Kawatani & Hamilton, 2013; Rao et al., 2020c). This weakening also includes an increased probability of disruptions to the QBO's regular evolution (Anstey et al., 2021), and indeed after more than 60 years of steady QBO evolution since regular observations began in 1953, two disruptions of the QBO have occurred in the past 10 years (Osprey et al., 2016; Wang et al., 2023) with the first disruption unpredicted and unexpected at the time. Nonetheless, there is substantial variability in QBO behavior from one cycle to the next which can lead to internal decadal variability, and this internal variability can mask any forced changes (Match & Fueglistaler, 2021b). Note that all of these

Table 1
The Number of Ensemble Members Available for Each Experiment Analyzed in this Paper

	LESFMIP model experiments					
	Hist-GHG	Hist-aer	Hist-volc	Hist-sol	Hist-totalO3	Reference
HadGEM3-GC31-LL	55	55	50	50	50	Andrews et al. (2020)
IPSL-CM6A-LR	10	10	–	–	–	Boucher et al. (2020)
MIROC6	50	10	10	10	10	Tatebe et al. (2019), Shiogama et al. (2023)
CNRM6.1	10	10	–	–	–	Voldoire et al. (2019)

Note. IPSL-CM6A-LR and CNRM6.1 have not made available hist-volc, hist-sol, and hist-totalO3 runs.

studies considered simulations in which all climate drivers are changing, and hence isolating the role of individual forcings (e.g., greenhouse gases, aerosols, or ozone) has not been possible.

The role of one specific climate external driver, namely explosive volcanic eruptions, for impacting QBO behavior has been studied by a few papers. A super-eruption can disrupt the QBO evolution and instead lead to persistent easterlies for five or more years (Brenna et al., 2021). More moderate eruptions such as Krakatoa and Pinatubo can bias the QBO toward a westerly state and lengthen the duration of westerly QBO (wQBO) phases while shortening easterly QBO (eQBO) phases, however the amplitude is mostly unchanged (DallaSanta et al., 2021). Brown et al. (2023) focus on the Tambora and Pinatubo eruptions and reach a somewhat similar conclusion—the QBO phase evolution is delayed—with the eQBO phase most strongly affected. These studies use small (six members at most) ensembles, however, and it is unclear whether these results are robust to internal variability. Finally, one study focused on the effect of the historical ozone forcing used for CMIP6 (Checa-Garcia, 2018; Checa-Garcia et al., 2018) on the QBO (Butchart et al., 2023), and they found that the ozone forcing likely leads to synchronization of the QBO phase across different ensemble members.

This paper revisits the role of five climate forcings—anthropogenic greenhouse gases, aerosols, ozone concentrations, volcanic eruptions, and solar variability—for changes in the structure of the QBO from 1850 to 2020. Specifically, a new Large Ensemble Single Forcing Model Intercomparison Project (LESFMIP) (Smith et al., 2022) has been organized using CMIP6 era models in order to isolate the impacts of different external drivers on the Earth system based on the hist-GHG, hist-aer, hist-totalO3, hist-volc, and hist-sol experiments, that correspond, respectively, to the five climate forcing specified above. These experiments form a bedrock of the analysis plan of the World Climate Research Program Lighthouse Activity on Explaining and Predicting Earth System Change (Findell et al., 2023). After introducing the LESFMIP data set in Section 2, we isolate the forced response of the QBO to greenhouse gases, aerosols, ozone, solar variability, and volcanic eruptions in Section 3, and finally discuss implications of the results in Section 4.

2. Methods

This paper focuses on models contributing to the LESFMIP project. Four of the LESFMIP models spontaneously simulate a QBO: HadGEM3-GC31-LL (Andrews et al., 2020), IPSL-CM6A-LR (Boucher et al., 2020), MIROC6 (Shiogama et al., 2023; Tatebe et al., 2019), and CNRM6.1 (Voldoire et al., 2019). We focus on five of the single forcing experiments included in Phase 1 of the LESFMIP protocol: hist-GHG, hist-aer, hist-volc, hist-solar, and hist-totalO3. For each of these, at least 10 ensemble members have been simulated over the period 1850–2020. The specific ensemble sizes for each run are shown in Table 1. Full details of the LESFMIP protocol can be found in Smith et al. (2022), but briefly, the forcings are those provided for CMIP6. The solar forcing is spectrally resolved and includes a solar signal in ozone, the volcano forcing also includes a signal in ozone, and the GHG forcing intentionally does not include any interannual, decadal, or centennial variability in ozone. The ozone forcing is described in Checa-Garcia et al. (2018) and Checa-Garcia (2018), and is based on two chemistry climate models validated against ozonesondes and satellite data. The data is freely available on the Earth System Grid Federation (ESGF).

While the large ensemble sizes available as part of LESFMIP allow for an isolation of the role of these five forcings for the QBO evolution, there is a downside: the data volume is huge (approximately 65,000 years of model output), and some diagnostics that one would like to analyze to understand why the QBO responds in the

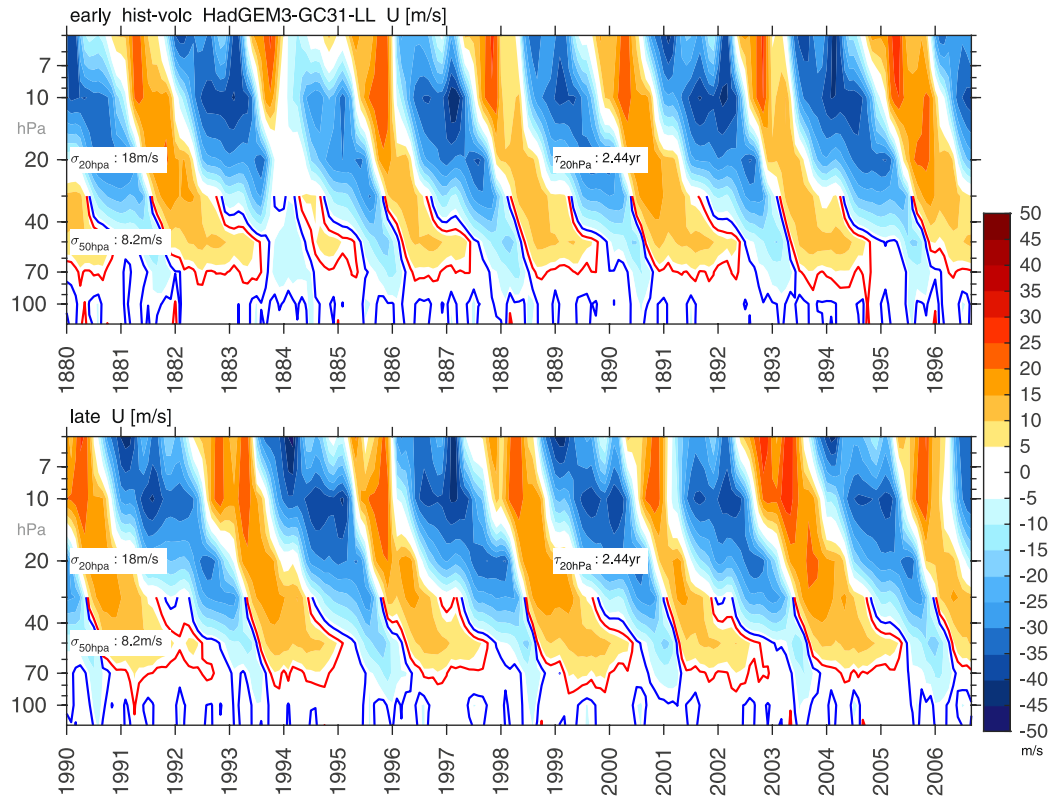

Figure 1. Zonal mean zonal wind from 5S to 5N in hist-volc for 1880–1997 and 1990–2007 for the first ensemble member of HadGEM3. The ±2.5 m/s contours are shown below 30 hPa. Note the weakening of the normal QBO evolution in early 1884 (and to a lesser degree in early 1992 below 30 hPa). Each panel also indicates the periodicity of the 20 hpa winds, and also the standard deviation (after subtracting the climatology) of the QBO winds at 20 and 50 hPa, averaged over all hist-volc ensemble members and computed over (top) 1850–1931 and (bottom) 1932–1979.

way it does are simply unavailable. For example, the transformed Eulerian mean vertical velocity ($\overline{w}^*$; Gerber & Manzini, 2016) is archived on ESGF for HadGEM3-GC31-LL only.

Monthly zonal mean zonal winds from 5°S to 5°N (U5S5N) are used to define the QBO. In order to provide a measure of the amplitude of the QBO and the possibility of disruption events at monthly resolution, we represent the QBO state in a two-dimensional phase space defined by the two leading principal components (PCs) of QBO winds from 70 to 10 hPa (Wallace et al., 1993). We perform the empirical orthogonal function (EOF) decomposition for each model separately, rather than regressing modeled zonal winds onto observed EOFs. This is because regressing onto observed EOFs would conflate biases in how a model represents the QBO with disruption events, thus offering a blurred picture of how each of the forcings affects disruption events. We define a disruption event as when $\sqrt{PC1^2 + PC2^2}$ drops below 40% of its climatological value over the entirety of all available simulations from that model (see Figure 3b of Wang et al., 2023, for the historical observed analog). This definition of a QBO disruption is agnostic to the specific dynamical processes leading to the disruption, and does not require that these disruption events resemble the particular dynamics of the observed disruptions in 2015/2016 and 2019/2020.

3. Results

All four models considered here simulate a spontaneous QBO. We demonstrate this by showing two 17-year snapshots of the QBO index for HadGEM3-GC31-LL (Figure 1), IPSL-CM6A-LR (Figure S1 in Supporting Information S1), MIROC6 (Figure S2 in Supporting Information S1), and CNRM6.1 (Figure S3 in Supporting Information S1). In order to quantify QBO amplitude in individual months, we perform a PC analysis of the U5S5N data and retain the two leading modes. Figure 2 shows an example of the evolution of the two leading modes for the first 16 ensemble members of the HadGEM3-GC31-LL hist-volc experiment. During a regular

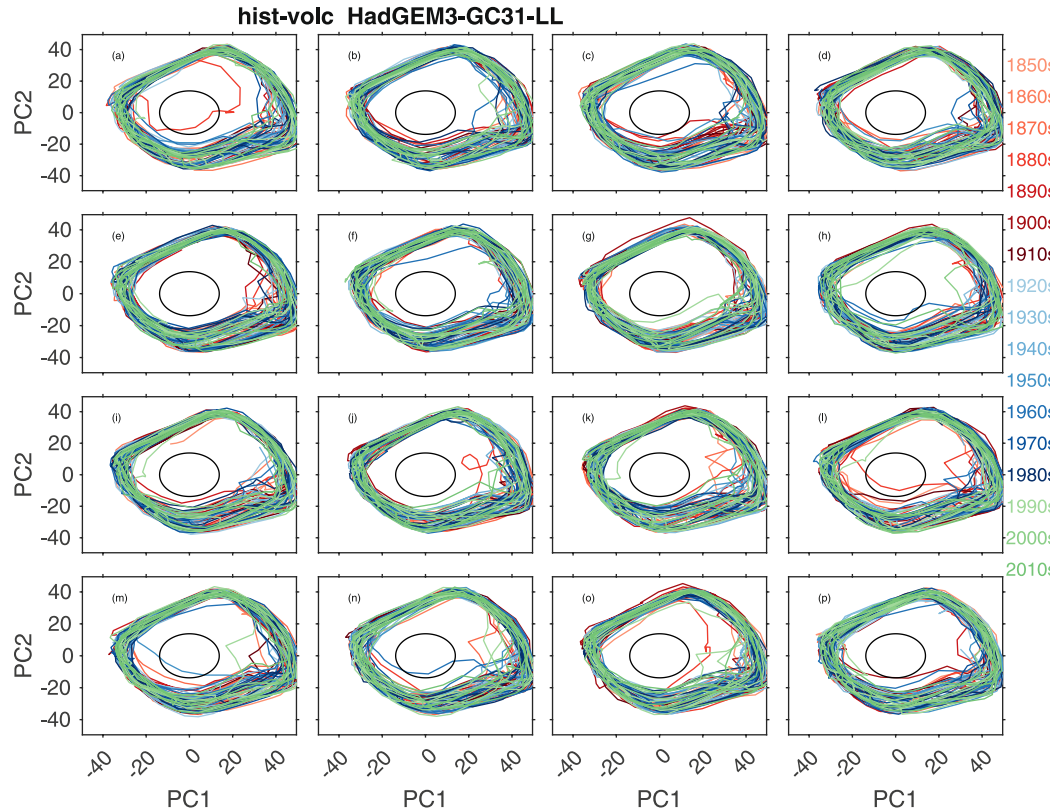

Figure 2. Example of QBO evolution in principle component phase space [units: m/s] for the first 16 of the 50 HadGEM3-GC31-LL ensemble members for hist-volc. Each panel shows a single ensemble member, and the evolution is color-coded by decade. We define a disruption event as occurring when $\sqrt{PC1^2 + PC2^2}$ drops below 40% of its climatological value, and this 40% threshold is indicated with a black circle. Note the disruption events in panels (a, l, m, n) in which the phase evolution approaches the origin. The disruption event in (a) is the same event shown in Figure 1a near 1884.

QBO cycle, one nearly circular loop is completed, and hence the distance from the center and rate of progress along the orbit provide a measure of the instantaneous amplitude and rate of phase progression of the QBO.

Figures similar to Figure 2 have been created for all ensemble members and all four models, and we then compute $\sqrt{PC1^2 + PC2^2}$ averaged across all available ensemble members. The ensemble mean of $\sqrt{PC1^2 + PC2^2}$, our metric of QBO amplitude with monthly resolution, is shown in Figure 3. There is a monotonic weakening of QBO amplitude in hist-GHG for all four models. For hist-aer, there is a strengthening for HadGEM3-GC31-LL and to a smaller extent for IPSL-CM6A-LR and CNRM6.1, but not for MIROC6. For hist-volc, there is a notable decline in QBO amplitude near 1883 and 1991, a feature we return to in Section 3.1. There is little discernible impact of solar variability on the QBO. The hist-totalO3 simulation will be discussed in Section 3.2.

While the PC decomposition of the QBO allows for an instantaneous metric of the QBO amplitude, it precludes an understanding of which stratospheric level(s) in particular feature a weakening of the QBO. Previous work has indicated that it is mainly the lower stratospheric QBO that weakens in response to increased GHG (Butchart et al., 2020; Rao et al., 2020c). We reconsider this effect by computing the standard deviation of winds at each pressure level over sliding 20-year windows, and then plotting the percentage decrease in QBO amplitude as compared to 1850–1870 in Figure 4. Weakening of the QBO is most pronounced at 50 or 70 hPa for all models in hist-GHG, and the weakening exceeds 20% of preindustrial values. While the QBO also weakens near 10 hPa, the weakening is by less than 10%. For hist-aer, the strengthening of the QBO in HadGEM, CNRM, and ISPL is most pronounced in the lower stratosphere as well. The gradual strengthening of $\overline{w}^*$ in hist-GHG and weakening of $\overline{w}^*$ in hist-aer is consistent with the simulated weakening and strengthening (respectively) of the QBO (Figures 5a and 5b; Watanabe & Kawatani, 2012). The opposing behavior of QBO amplitude in hist-GHG and hist-aer is also consistent with the relative shifts in tropopause height and tropospheric expansion in response to these forcings

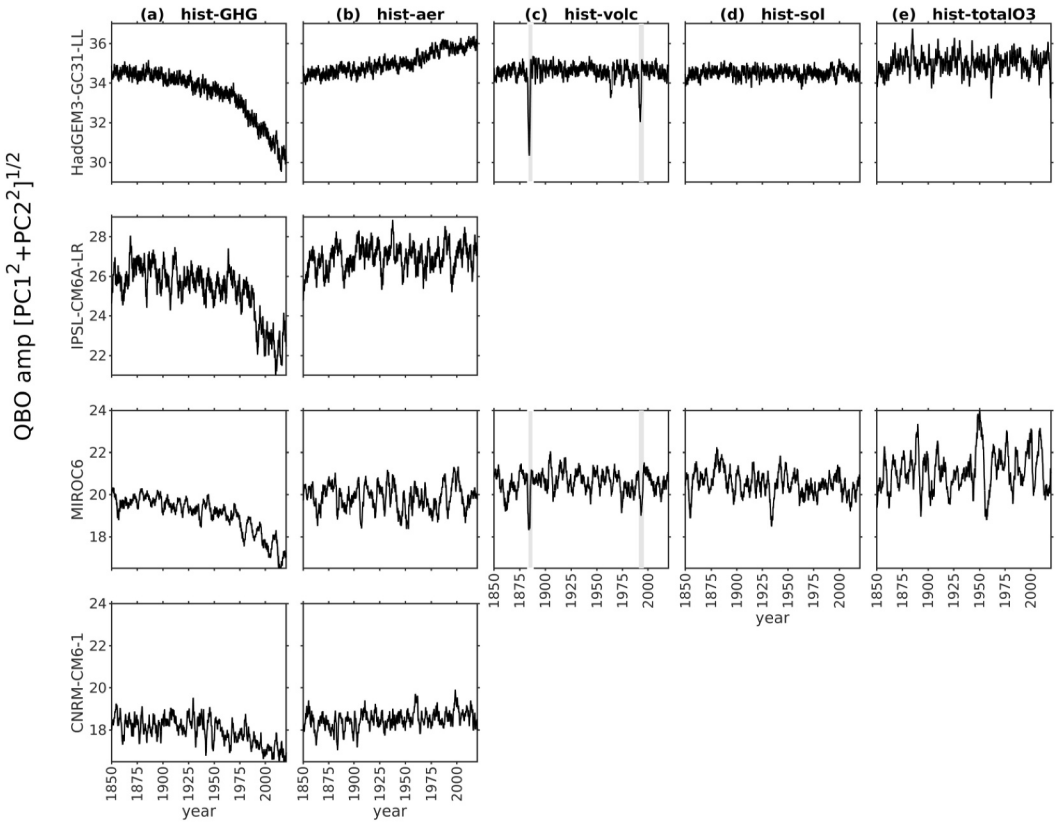

Figure 3. Evolution of QBO amplitude ($\sqrt{PC1^2 + PC2^2}$; m/s) for the five single forcing large ensembles for (top) HadGEM3-GC31-LL, (second) IPSL-CM6A-LR, (third) MIROC6, and (bottom) CNRM-CM6-1. The QBO amplitude is computed for each ensemble member, smoothed with a 28-month running mean to remove any dependence on the QBO phase, and then averaged across all available ensemble members. Gray shading for hist-volc indicates the years 1883–1888 and 1991–1996.

(Match & Fueglistaler, 2021b; Oberländer-Hayn et al., 2016; Santer et al., 2003), an issue we return to in Section 4.

These changes in QBO amplitude raise the interesting possibility that these five external forcings may also affect the likelihood of disruption events, and the large data volume available in the LESFMIP archive—a factor of 1,000 more than is available in observations—allows for a statistically robust examination of this possibility. During a disruption the first two PCs no longer explain most of the variance of tropical winds, and in PC1/PC2 phase space this corresponds to $\sqrt{PC1^2 + PC2^2}$ dropping well below typical values (for this paper we use a threshold of 40% of its time-mean value). Such an event occurred in the 1880s in the first ensemble member of hist-volc in HadGEM3-GC31-LL (Figure 2a), a feature also evident in Figure 1.

A histogram of the number of months of data in which this criteria is met for each decade is shown in Figure 6. (Note that for this figure, we count all months in which this criteria is met and not just the onset month, though the relative number of disrupted months per decade as compared to other decades is similar if we consider just the onset.) For the first three models, higher GHG concentrations lead to a clear increase in the number of disrupted QBOs. Furthermore, there are notably more disrupted QBO events for hist-volc in the 1880s for HadGEM3-GC31-LL and in the 1990s for MIROC6. Nonetheless, QBO disruption events happen (though very infrequently) even without favorable external forcings. Specifically, 6 QBO disruption events occurred in HadGEM3-GC31-LL hist-GHG from 1850 to 1900, and thus 0.22% of available models years feature a disruption (6 events in 2,750 years of model output). In contrast, 19 occurred from 2000 to 2020 (1.7% of available models years), and so elevated GHG concentrations leads to approximately a tenfold increase in the likelihood of a disruption event occurring. Nonetheless, the probability of occurrence in HadGEM3-GC31-LL since 2000 is less than the observed frequency of 2 events in 24 years, or 8%. This does not necessarily imply a model discrepancy, as

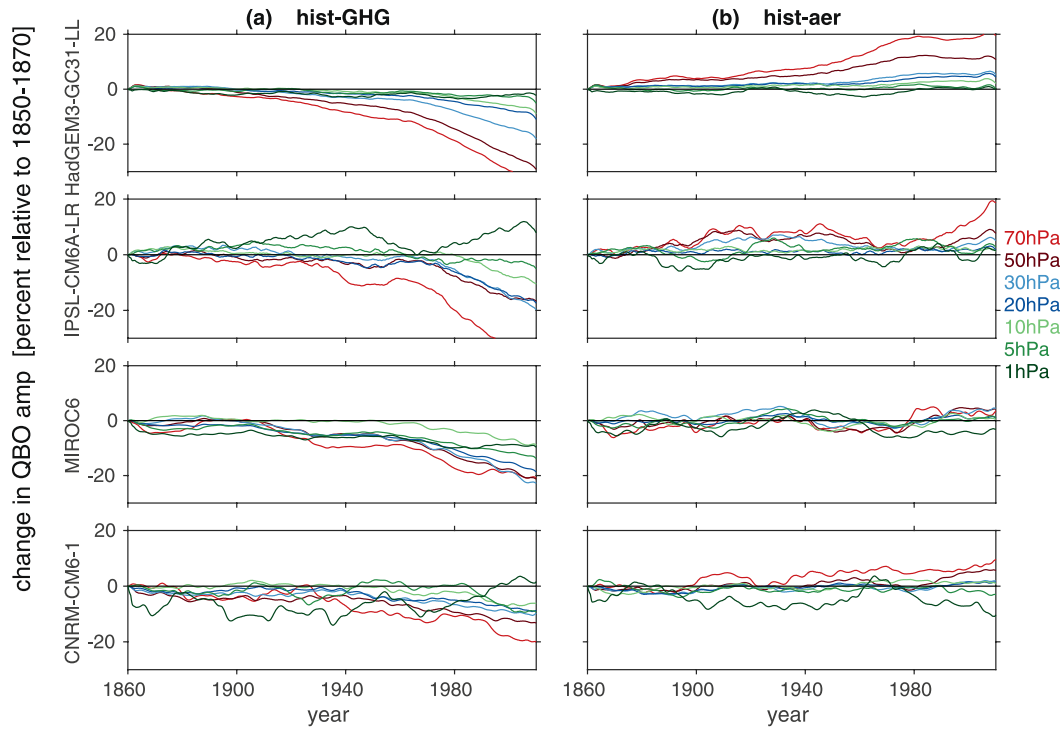

Figure 4. Evolution of the change in QBO amplitude at each pressure level relative to the 1850–1870 base period for (top) HadGEM3-GC31-LL, (second) IPSL-CM6A-LR, (third) MIROC6, and (bottom) CNRM-CM6-1. The amplitude is quantified as the standard deviation of rolling 20-year timeslices of data. Taking 1900–1920 as an example, we show $100 \times \frac{\sigma_{[1900-1920]} - \sigma_{[1850-1870]}}{\sigma_{[1850-1870]}}$.

individual HadGEM3-GC31-LL hist-GHG members simulate 2 disruptions since 2000, and 3 since 1980 (e.g., Figure S4 in Supporting Information S1).

The observed 2016 and 2020 disruption events began in early boreal spring: in PC1/PC2 phase space, the inward spiral toward the origin occurred in March in both cases (see Figure 3b of Wang et al., 2023). This raises the question of whether there is a preferred season for the QBO be disrupted. We consider this by computing the onset month of each QBO disruption (i.e., the first month in which $\sqrt{PC1^2 + PC2^2}$ drops below 40% of its climatological value), and then plot a histogram of onset month in Figure 7. For all models, most disruption events onset in the boreal late winter or early spring. (MIROC6 has an additional, secondary peak in boreal summer.) This seasonality in the models matches the observed seasonality for the two observed events. Note that this seasonality does not match the seasonality of climatological $\sqrt{PC1^2 + PC2^2}$, which shows a minima in June for HadGEM3-GC31-LL, in January for MIROC6 and IPSL-CM6A-LR, and in April for CNRM6.1. Hence, it appears that the QBO is more prone to disruption in late boreal winter or early spring in both observations and models.

Finally, we consider which phase of the QBO is most likely to be disrupted. Specifically, Figure 8 shows the time versus height evolution of tropical winds for all events in which $\sqrt{PC1^2 + PC2^2}$ drops below 30% of its

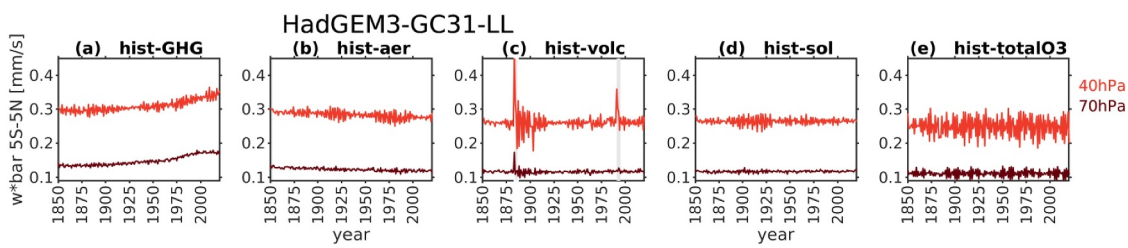

Figure 5. Time evolution of annual averaged $\overline{w}^*$ in HadGEM at 40 and 70 hPa. The necessary data for this computation is available on ESGF for HadGEM only.

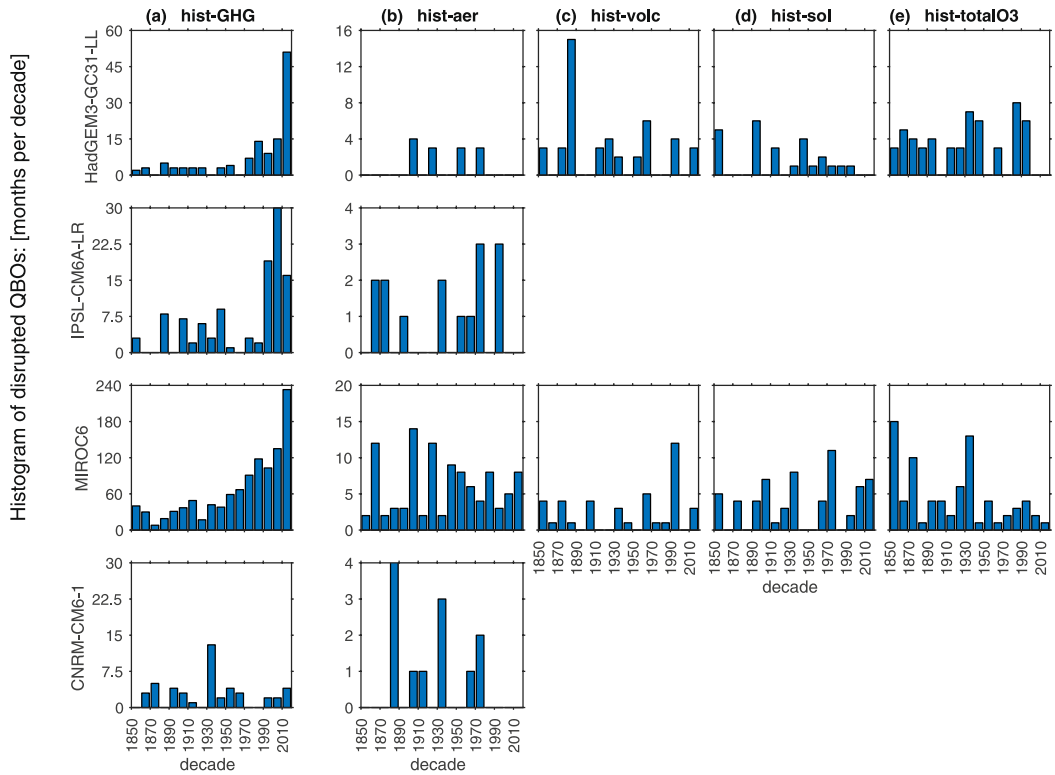

Figure 6. Histogram of the decades in which a disruption event occurred for (top) HadGEM3-GC31-LL, (second) IPSL-CM6A-LR, (third) MIROC6, and (bottom) CNRM-CM6-1. All available ensemble members are included, and we sum over all ensemble members. A disruption event is defined as when $\sqrt{PC1^2 + PC2^2}$ drops below 40% of its climatological value, and the corresponding values for each model are: HadGEM3-GC31-LL (14 m/s), IPSL (10 m/s), MIROC6 (8 m/s), and CNRM-CM6-1 (7 m/s). Hist-GHG is in the first column, hist-aer in the second column, hist-volc in the third column, hist-sol in the fourth column, and hist-totalO3 in the fifth column.

climatological value in hist-GHG of HadGEM3-GC31-LL; that is, we use a stricter threshold to ease visualization and reduce the number of panels. We begin 8 months before $\sqrt{PC1^2 + PC2^2}$ drops below 30% of its climatological value, and continue for 8 months after. Note that all of these simulated disruption events were more impactful than either of the two observed events: for most of the modeled events, the QBO completely disappeared for a few months, before gradually re-establishing easterlies near 20 hPa. Nearly all disruption events are preceded by the QBO regime with westerlies in the upper stratosphere and easterlies in the lower stratosphere (Figure 8e is the lone possible exception, as its westerlies peak slightly lower than the rest of the events.). Generally similar results are evident for disruption events in MIROC6 (Figure S5 in Supporting Information S1). This phase resembles that observed in mid 2015, however in 2019 the QBO wind regime was somewhat different. To recover a phase evolution that resembles what occurred in late 2019, we need to include more moderate modeled disruption events ($\sqrt{PC1^2 + PC2^2}$ between 30% and 40% of its climatological value; not shown for visual conciseness). The 2015/2016 event featured upward propagation of a thin westerly jet within an easterly regime, and while we find such behavior occasionally in response to a volcanic eruption (an effect that we will describe in Section 3.1), none of the cases with time varying GHGs only show such behavior. A further difference is that for the two observed cases, a "dent" in the westerlies occurred below 40 hPa; in most of the HadGEM and MIROC6 disruptions there is not a well-formed dent, but rather a complete elimination of the westerlies. Nonetheless a "dent" in the westerlies does occur in a few cases (Figures 8a, 8p, and 8s, Figure S5o in Supporting Information S1), but it is found higher up, near 20 hPa.

3.1. A Closer Look at the Effect of the Pinatubo and Krakatoa Eruptions on the QBO in Hist-Volc

Both MIROC6 and HadGEM3-GC31-LL indicate that volcanic eruptions lead to a weakening of the QBO (Figure 3) and a greater likelihood for a disruption (Figure 6). HadGEM3 also simulates a weakening of the QBO

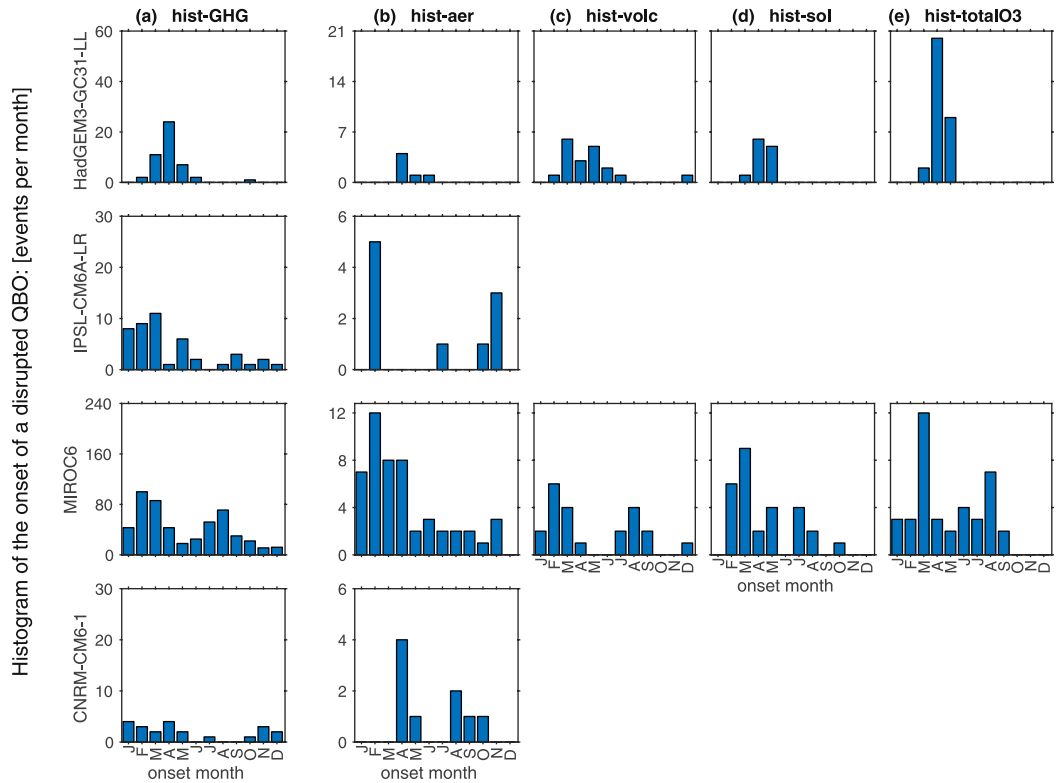

Figure 7. As in Figure 6, but showing the month for the onset of each disruption event.

and an increase of disruption events after Agung erupted in 1963; in the smaller MIRCO6 ensemble, it is hard to isolate a similar effect though there is an indication of a delayed weakening later in the 1960s. Previous work using single models and small ensemble sizes has shown that the impact of volcanic eruptions on the QBO also depends on the preceding QBO phase (Brown et al., 2023; DallaSanta et al., 2021). The LESFMIP models allow us to revisit these studies by considering the effect of the eruption of Pinatubo and Krakatoa on each of four

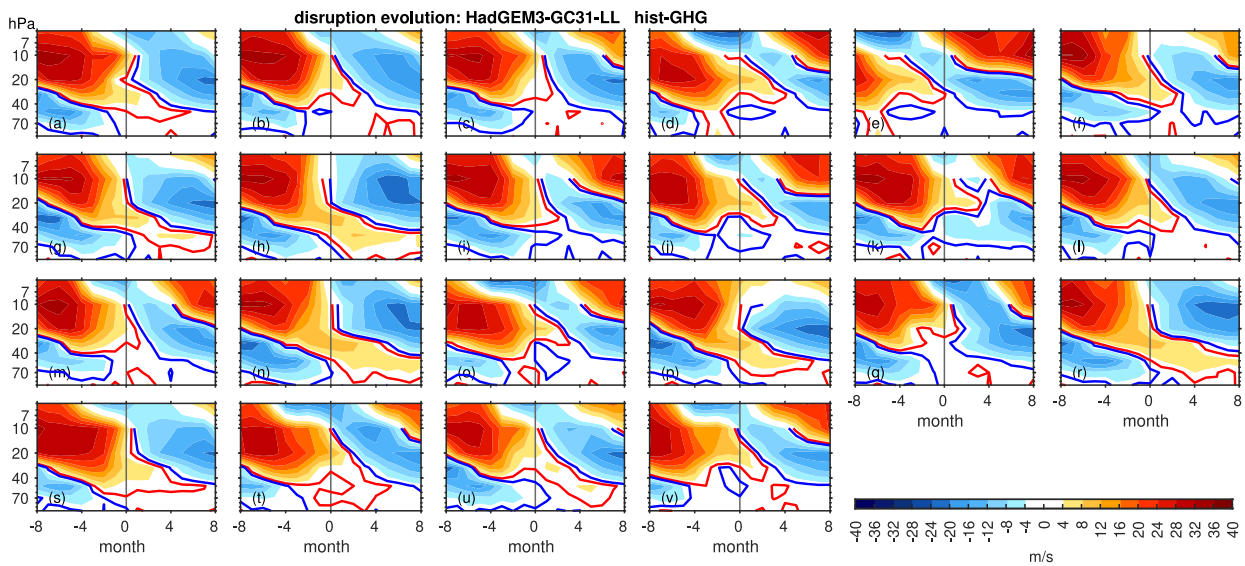

Figure 8. Time-height evolution of U5N-5S for the disruption events in which $\sqrt{PC1^2 + PC2^2}$ drops below 30% of its climatological value in HadGEM3-GC31-LL in the hist-GHG integrations. We show from 8 months before the disruption onset to 8 months after onset to capture the full lifecycle. The isotach of ±1.5m/s is shown in red and blue below 10 hPa. The 22 panels correspond to the 22 distinct events. A comparable figure but for MIROC6 is in Figure S5 in Supporting Information S1.

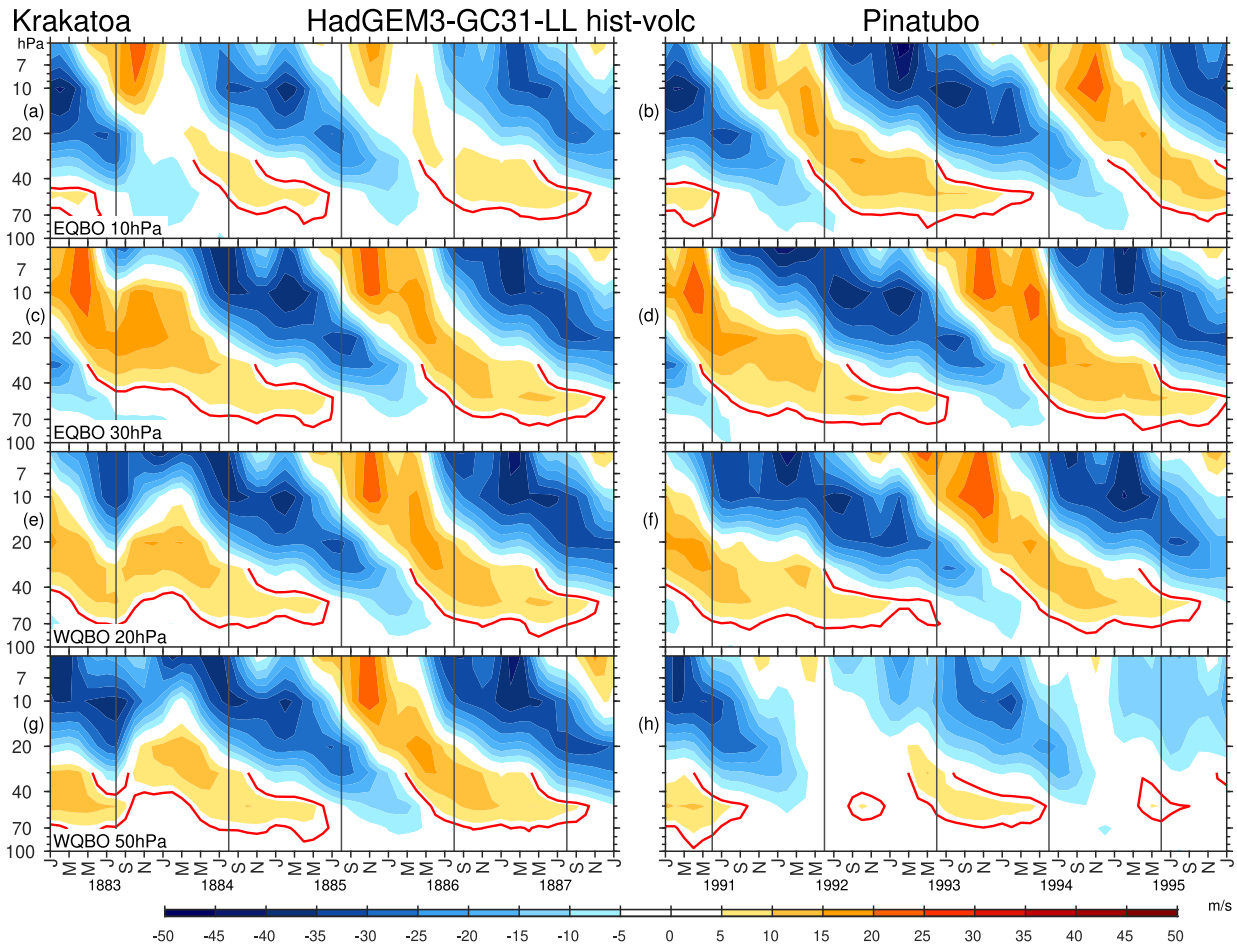

Figure 9. Time-height evolution of U5N-5S for HadGEM3-GC31-LL from 1883 to 1887 and 1991 to 1995 in the hist-volc integrations, for the five ensemble members with strongest (a, b) easterlies at 10 hPa; (c, d) easterlies at 30 hPa; (e, f) westerlies at 20 hPa; (g, h) westerlies at 50 hPa in January before the eruption. The first vertical line indicates the eruption month (June 1991 and August 1883), and subsequent vertical lines follow in 12-month intervals. The isotach of 2.5 m/s is shown in red below 30 hPa. The analogous figure but for hist-GHG (in which there was no volcanic eruption) is in Figure S6 in Supporting Information S1.

different QBO phases for two different models (HadGEM3-GC31-LL in Figure 9, and MIROC6 in Figure 10). Analogous figure but for hist-GHG (in which there was no volcanic eruption) are in Figures S6 and S7 in Supporting Information S1. We first discuss the responses in each model for each phase, then assess which aspects of the response are robust to both models, and finally compare to previous work.

We begin by considering the response of the QBO phase with easterlies at 10 hPa in HadGEM3-GC31-LL to Pinatubo and Krakatoa. Specifically, we composite U5N-5S for HadGEM3-GC31-LL from 1883 to 1887 and 1991 to 1995, isolate the five ensemble members with strongest easterlies at 10 hPa in the January before the eruption, and then compute the composite mean QBO evolution for these five members (Figures 9a and 9b). We choose five members with strongest winds to ensure a similar QBO phase structure, and results are similar if we choose four or six. After the major eruption in August 1883, the QBO lower stratospheric easterlies weaken dramatically, and in January 1884 the QBO is fully disrupted. By summer of 1884, however, the QBO phase evolution has resumed its normal course. The 1991 eruption of Pinatubo has a minimal impact on this QBO phase, however the mid-stratospheric westerlies in the winter of 1991/1992 in Figure 9b are weakened as compared to Figure S6b in Supporting Information S1. Next, we consider the response to eruptions for the five ensemble members with strongest easterlies at 30 hPa in the January before the eruption (Figures 9c and 9d), the phase with QBO easterlies present throughout the mid and lower stratosphere. The regular evolution of QBO winds is not affected by either Pinatubo or Krakatoa, however the westerly phase in the lower stratosphere following the eruption persists for nearly 2 years, with the effect particularly noticeable after Pinatubo. Next, we consider the five ensemble members with strongest westerlies at 20 hPa in the January before the eruption (Figures 9e and 9f).

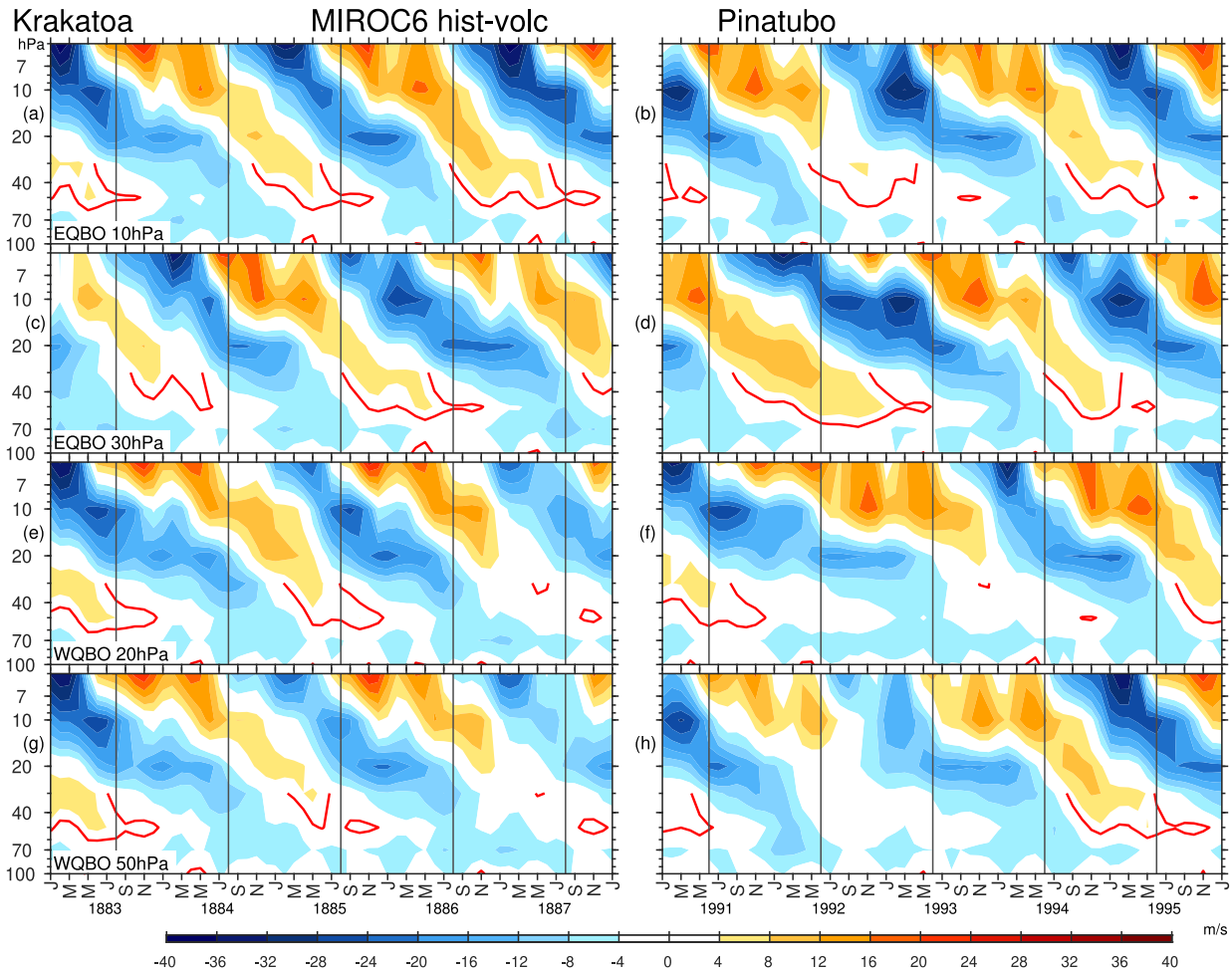

Figure 10. As in Figure 9 but for MIROC6 and for the two ensemble members with strongest winds at each level. The isotach of 1.75 m/s is shown in red below 30 hPa. The analogous figure but for hist-GHG (in which there was no volcanic eruption) is in Figure S7 in Supporting Information S1.

The extension in the duration of QBO westerly is particularly pronounced in response to Krakatoa (contrast Figures 9e and 9f with Figures S6e and S6f in Supporting Information S1). This effect, in many ways, mimics an upward jump in the QBO westerly winds by ∼30hPa immediately after the eruption. This upward jump is even more pronounced for the five members with westerlies at 50 hPa in the January before the eruption (Figures 9g and 9h), especially for Krakatoa. For this QBO phase, Pinatubo leads to a complete disruption of the QBO in spring of 1992. This effect appear to be consistent with the strong impact that volcanic eruptions have on $\overline{w}^*$ in these runs (Figure 5c) at 70 hPa and especially at 40 hPa. This acceleration of $\overline{w}^*$ enhances the $\overline{w}^* \frac{\partial u}{\partial z}$ term in the zonal momentum budget, and can lead to upward jumps or stalling of QBO winds (cf. Brown et al., 2023).

The sensitivities are somewhat different for MIROC6. Specifically, Figure 10 is the equivalent of Figure 9 but for MIROC6, and we include the two members with strongest winds at each level (note that there are only 10 hist-volc members for MIROC6). The eruption of Pinatubo led to a prolonged westerly phase in the mid- and lower-stratosphere for members with strong easterlies at 30 hPa before the eruption (Figure 10d), and to a lesser degree for other phases. Pinatubo also tends to induce disruptions of the QBO a year after eruption for QBO phases with easterlies at 10 hPa or westerlies at 50 hPa before eruption (Figures 10b and 10h). Krakatoa does not have a noticeable effect on QBO disruptions in MIROC6 (see also Figure 6), however the QBO winds are still weaker in Figures 10c and 10e than in corresponding panels in Figure S7 in Supporting Information S1.

Of these various effects, the only ones that are common to both MIROC6 and HadGEM3-GC31-LL is that Pinatubo is more likely to lead to a disruption if preceded by the QBO phase with westerlies at 50 hPa (Figures 9h and 10h), and that Pinatubo leads to a prolonging of mid-to lower-stratospheric westerlies (westerlies at 40 to

60 hPa in Figures 9d and 10d persist for 2 years). This prolongation of mid-and lower-stratospheric westerlies is consistent with the results of DallaSanta et al. (2021) and Brown et al. (2023) who examined different models than those contributing to the LESFMIP, and hence the lengthening of westerlies from 40 to 60 hPa appears to be robust. These earlier studies did not consider QBO disruptions.

Overall, volcanic eruptions have a short-lived (<5 years) but pronounced impact on the QBO period, amplitude, and propensity for disruption.

3.2. Effect of Ozone on the QBO

We now turn our attention to the hist-totalO3 runs. While decadal-scale changes in the concentrations of ozone depleting substances had little impact on the QBO, there is increased variance in QBO winds as compared to the other simulations (Figure 3e). This effect is most pronounced in the mid-and lower-stratosphere (figure not shown). Specifically, we quantify this by computing the variance for each individual run and then averaging the variance across all members for individual experiments. The variance of 50 hPa U5S5N is 6.5% stronger in hist-totalO3 than in hist-solar in HadGEM3-GC31-LL, and 11% stronger in MIROC6. At 20 hPa, this increase in variance is 2.8% and 3.4% respectively. A similar increase is also evident if we compare hist-totalO3 to any of the other simulations. It is difficult to diagnose why variance increases and overall QBO amplitude grows given the output available on ESGF, however we note that there is a similar increase in variance for $\overline{w}^*$ for the one model that made it available (Figure 5e). A detailed study of ozone-QBO feedback processes is beyond the scope of this study. Shibata (2021) recently found that stronger ozone feedbacks in the coupled chemistry model MRI-CCM leads to a longer QBO periodicity. We find that the QBO period is shortest in hist-totalO3 by 8% in HadGEM3-GC31-LL (2.5–2.3 years), and by 5% in MIROC6 (2.07–1.95 years), however these models do not internally generate the ozone field.

The historical CMIP6 ozone forcing includes a QBO signal, which has been shown to lead to synchronization of the QBO phase across different ensemble members (Butchart et al., 2023). The ensemble sizes considered by Butchart et al. (2023) were relatively small and all historical forcings were time varying (not just ozone), so it was not possible to isolate the role of ozone in Butchart et al. (2023). To test whether this effect is evident in the LESFMIP runs, we adopt the following methodology to quantify phase synchronization:

1. Apply a 5th order butterworth bandpass filter with cuts at 14 and 40 months to the U5S-5N data of each ensemble member (hereafter $\widetilde{Ueq}_k$) and of the ensemble mean of the available ensemble members of a given experiment in each model. This filtering helps isolate the characteristic QBO timescale.
2. Compute the standard deviation of $\widetilde{Ueq}$ from step 1, both of the ensemble means $\left(\widetilde{Ueq}EM\right)$ and also of each individual member $\left(\widetilde{Ueq}_{k=1\ldots N}\right)$ for each of the N members.
3. Contrast the standard deviation of the ensemble mean $\widetilde{Ueq}$ (i.e., the QBO amplitude of the ensemble mean) with the mean of the standard deviation for all available members (i.e., the QBO amplitude of an average ensemble member).

The above steps are repeated for levels from 70 to 1 hpa and for both models with all five scenarios. Note that if the phase is unsychronized, $\widetilde{Ueq}EM$ will equal zero for a sufficiently large ensemble, and hence the QBO amplitude of the ensemble mean will also equal zero. We then display the QBO amplitude of the ensemble mean relative to that in each individual member as a percentage in Figure 11, which shows the resulting phase synchronization for each run.

There is clearly more synchronization for hist-totalO3 than for the other four scenarios. The synchronization exceeds 50% at both levels and for both models (similar to Butchart et al., 2023). There is generally more synchronization for MIROC6 than HadGEM3-GC31-LL; however, the larger ensemble sizes in HadGEM3-GC31-LL are responsible for this effect (confirmed by subsampling HadGEM3-GC31-LL to match the ensemble sizes in MIROC6). This effect is confirmed by examining the 1850–2020 QBO time series inferred from the ensemble-mean winds (not shown). A similar, though far weaker, synchronization is evident in hist-volc for HadGEM3-GC31-LL; this synchronization is visually apparent in 1885, 1886, and 1887 in the left column of Figure 9, whereby ensemble members with very different QBO phases in January 1883 show the same QBO phase 2 years later and beyond. For MIROC6, hist-sol, and to a lesser degree hist-volc, leads to synchronization. Overall, we confirm the conclusion of Butchart et al. (2023) that the phase synchronization of the QBO across CMIP models is due to the use of historical time varying ozone; this is a stronger conclusion than that reached by

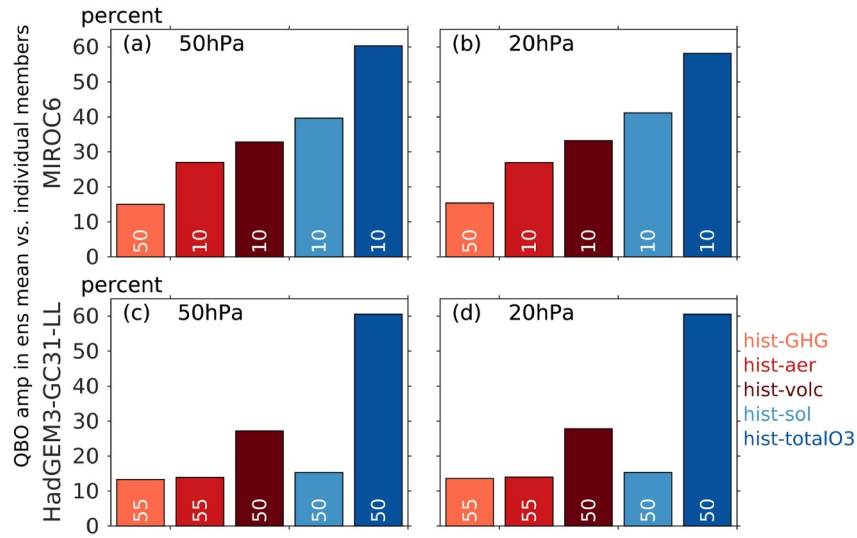

Figure 11. The synchronization of the QBO in the ensemble mean at 20 and 50 hPa for the two models with all five scenarios. The synchronization is quantified by first applying a 14–40 months bandpass filter to U5S5N to isolate QBO timescales, and then comparing the standard deviation of the ensemble mean U5S5N to the standard deviation for all available members (ranges from 10 to 55 depending on model and scenario, indicated in each bar).

Butchart et al. (2023) who analyzed simulations with all historical forcings time varying. Nonetheless, we acknowledge that the ozone only experiment also includes tropospheric ozone variability, and hence we cannot isolate the role of stratospheric ozone for the phase synchronization.

3.3. Effect of the External Forcings on QBO Period

While our primary focus has been on QBO amplitude and disruption events, previous work has noted that increased GHGs leads to a shortening of QBO period in many models (Butchart et al., 2020; Rao et al., 2020c), though not in others (Richter et al., 2022). We quantify this by computing the time to complete a complete orbit in PC1 and PC2 phase space averaged across all available ensemble members. Specifically, we first compute the change in the phase angle of the QBO in PC1/PC2 phase space from each month to the one following, and then apply a 36-month running mean to remove dependency on QBO phase and the annual cycle. We then average the changes in phase angle across all available ensemble members, and display the resulting periodicity for a complete cycle in Figure 12.

Increased GHGs leads to a longer period in two models (MIROC6 and IPSL), no change in HadGEM3, and a decrease in period in CNRM. Changes in the hist-aer runs are generally weaker, with a slight decrease in period in IPSL and an increase in CNRM. As discussed in Section 3.1, Krakatoa and Pinatubo led to stalling of the QBO. Solar variability has no detectable impact on the QBO period (in general agreement with Fischer & Tung, 2008; Kuai et al., 2009). Ozone variability tends to "fix" the slightly too-long period in HadGEM3, likely a byproduct of the phase synchronization discussed in Section 3.2. Results are similar if we apply a spectral analysis to the, say, 20 hPa 5S–5N winds for each ensemble member for data chunks in the beginning versus the end of the simulations (not shown). Overall, changes in the QBO period are generally not robust across models, except for the lengthening and stalling of the QBO after volcanic eruptions. In contrast, changes in QBO amplitude are more robust both in the LESFMIP models and in QBOi models (Richter et al., 2022).

4. Discussion and Conclusions

The Quasi-Biennial Oscillation is one of the most regular phenomena in the climate system not directly linked to variations in insolation, and from the start of regular observations in 1953 until 2015, the QBO phase evolution proceeded without interruption. Since 2015, two disruption events have occurred. The role of climate change for this clustering of disruption events is not clear, and is a primary motivation for this study. Namely, we explore the role of five key climate forcings—anthropogenic greenhouse gases, aerosols, ozone concentrations, volcanic

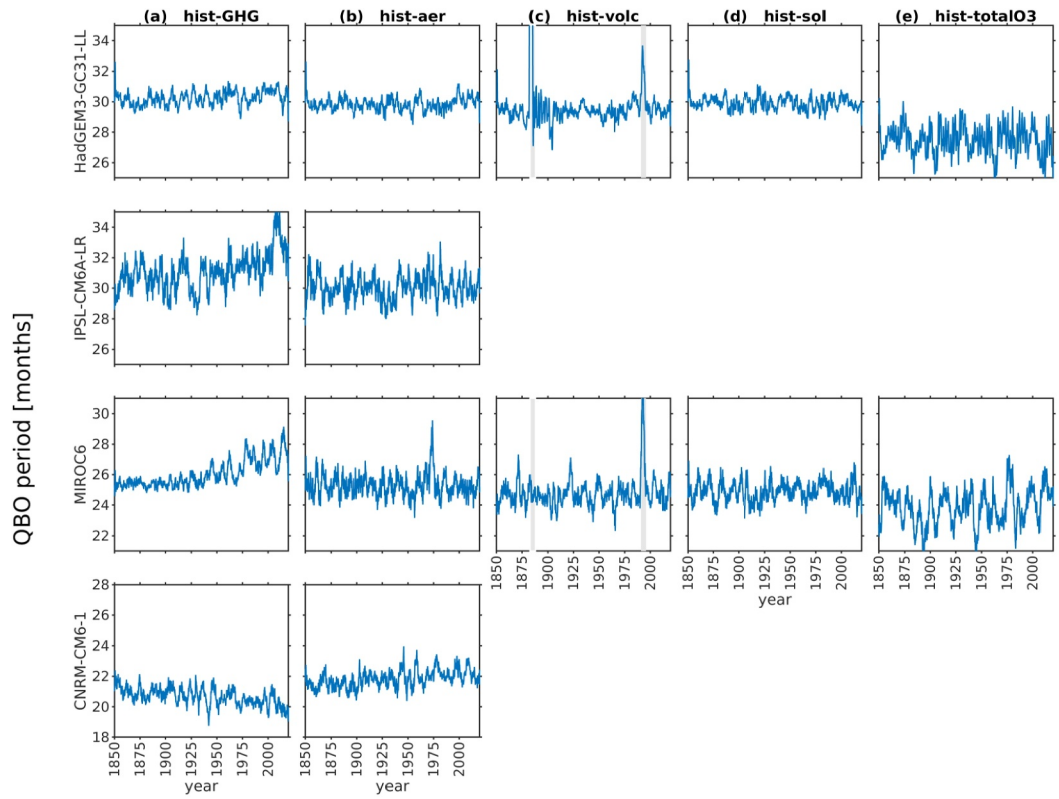

Figure 12. Evolution of QBO periodicity for the five single forcing large ensembles for (top) HadGEM3-GC31-LL, (second) IPSL-CM6A-LR, (third) MIROC6, and (bottom) CNRM-CM6-1. After computing the PCs for each ensemble member, we quantify the difference in the phase angle from 1 month to the next and then smooth with a 36-month running mean to remove any dependence on the QBO phase or the annual cycle. We then average across all available ensemble members, before converting the units to months per complete orbit in PC1/PC2 phase space. Gray shading for hist-volc indicates the years 1883–1888 and 1991–1996.

eruptions, and solar variability—for QBO amplitude and disruptions. For each of these five forcings, we examine at least 7,200 years of model output (~65,000 years in total) in which only that forcing is time varying. This allows for the isolation of weak signals that are usually hidden by internal variability.

Of these forcings, increasing greenhouse gas concentrations have the biggest long-term effect. Increasing GHG leads to a weakening of the QBO, especially in the lower stratosphere (Figures 3 and 4), and to a tenfold increase in the likelihood of disruption events (Figure 6). A decline in QBO amplitude has been noted in historical CMIP simulations with all forcings time varying (Butchart et al., 2020; Rao et al., 2020c), and the results shown here allow us to attribute this change to GHGs.

Increased aerosol concentrations lead to a small strengthening of the QBO in three of the four models and therefore helped mitigate the effect of GHGs on the QBO during the historical period (Figures 3 and 4). This implies that the weakening of the QBO in historical CMIP simulations with all forcings varying in time (Butchart et al., 2020; Rao et al., 2020c) likely underestimates the impact of GHGs.

Explosive volcanic eruptions (e.g., Pinatubo in 1991 or Krakatoa in 1883) have short-lived but strong impacts on the QBO. The QBO amplitude declines abruptly (Figure 3), the probability of a disruption event increases (Figure 6), and prolonged westerlies often follow in the lower- and mid-stratospheric (Figure 9). Krakatoa can also lead to the synchronization of the QBO phase (see left column of Figures 9 and 11). This prolongation of mid- and lower-stratospheric westerlies is consistent with previous work (Brown et al., 2023; DallaSanta et al., 2021).

Time varying ozone concentrations leads to pronounced synchronization of QBO phase across different members, consistent with Butchart et al. (2023), but we are able to better attribute it to ozone by contrasting the synchronization in simulations with just ozone time varying with simulations with other forcings time varying.

Furthermore, time varying ozone also leads to an increased amplitude of the QBO. A possible, speculative mechanism as to why is that lower ozone concentrations in the lowermost stratosphere (typically forced by eQBO at 50 hPa due to enhanced $\overline{w}^*$, but here imposed) will lead to reduced UV heating, and this will be dominantly balanced by a secondary circulation (Ming et al., 2016) which then perturbs the QBO momentum budget by altering vertical advection. In addition, reduced UV heating could also strengthen the cold anomalies already present during the QBO phase with easterlies in the lower stratosphere. This cooling then implies even stronger vertical shear of the QBO winds, and hence a stronger QBO, by thermal wind balance. Potential evidence for these effects is visible in $\overline{w}^*$ for the one model which makes it available (Figure 5e): $\overline{w}^*$ is more variable in the mid- or lower- stratosphere on sub-decadal timescales in totO3 than in the other experiments. Diagnosing this effect more directly is left for future work.

We were unable to identify any robust response of the QBO to solar variability. Solar variability directly impacts radiative heating and the Brewer-Dobson circulation near the stratopause, however the existence of a lower stratospheric response of the Brewer-Dobson circulation to solar variability is unclear (Chiodo et al., 2014; Givon et al., 2021; Kuchar et al., 2017); if there was to be an impact of solar variability on the lower- or mid- stratospheric Brewer-Dobson circulation, then an impact on the QBO would be expected. Ongoing work is devoted to more fully understanding the solar-only experiments.

The huge amount of data available also allows us to characterize the QBO phases that are most prone to disruption events. Disruption events are much more likely to onset in late boreal winter and early boreal spring (Figure 7). This matches the onset months of the observed 2016 and 2020 events: in PC1/PC2 phase space, the inward spiral toward the origin breached ~40% of the typical values of $\sqrt{PC1^2 + PC2^2}$ in around March in both cases (see Figure 3b of Wang et al., 2023). Two possible speculative explanations for this seasonality are that (a) tropical $\overline{w}^*$ is particularly strong in this season, and hence can lead to stalling of QBO phases and a lack of downward propagation; (b) extratropical Rossby waves are particularly strong in this season, and the likelihood of a pulse of extratropical Rossby waves impinging on the QBO is correspondingly larger. Future work should explore these possibilities.

Nearly all of the disruption events in these models are preceded 8 months before the disruption by the QBO phase with westerlies in the upper stratosphere and easterlies in the lower stratosphere (Figure 8). This phase resembles that observed in mid-2015 8 months before the first disruption event, and to a lesser degree the phase in late 2019 before the second event. The tendency for upper stratospheric westerlies and lower stratospheric easterlies to precede most disruptions can be understood using the heuristic model of Match and Fueglistaler (2021a). If a disruption is triggered by the formation of easterly winds embedded within westerlies, then the triggered shear zone should only start to amplify due to the QBO wave driving once there are no easterly winds below the triggering. This reduces to the condition that there be westerly winds everywhere below the triggering level. Thus, the conditions "preceding" the disruption would tend to be westerly winds in the lower stratosphere and the recent annihilation of an easterly wind region, whose annihilation permits the waves that used to dissipate there to now propagate upwards and amplify any triggered easterly winds from, say, laterally propagating waves. This appears to be what happens for most of the disruptions in Figure 8, where the onset of the disruptions (month = 0) tends to be shortly after the annihilation of the easterly winds at the bottom of the QBO. The importance of lowermost stratospheric westerlies immediately before the disruption was also emphasized by Kang et al. (2022).

Nonetheless, the details of the modeled disruption events do not closely resemble the particular nature of either disruption event (Figure 8). This inability to capture the details is perhaps to be expected, however, from the current generation of models: reanalysis systems relied on large assimilation increments to reproduce the 2015/2016 disruption (Match & Fueglistaler, 2021a), and most modeled QBOs still rely heavily on gravity wave parameterizations for most of the wave driving (e.g., Bushell et al., 2022). It seems possible that disruptions could move the QBO into a configuration where existing gravity wave parameterizations struggle to prognose the correct behavior, and even if a model produces a realistic basic state QBO, that does not guarantee that it will produce a realistic disrupted QBO. Finally, we attempted to isolate a precursor in $\overline{w}^*$ to HadGEM3 disruption events, however we were unable to isolate any effect due to the relationship between the QBO, its mean-meridional circulation, and $\overline{w}^*$ (Baldwin et al., 2001).

Little long-term change in QBO period is seen in any of the simulations. Note that none of the four models examined here have robust changes in QBO period in CMIP6 future simulations either (Butchart et al., 2020; Rao

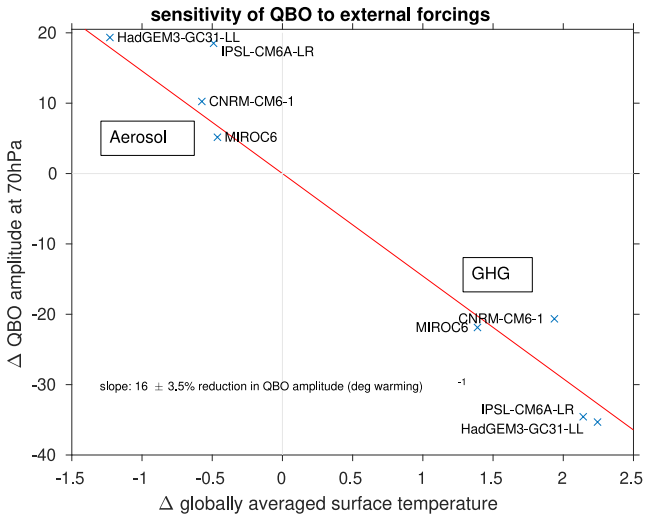

Figure 13. A comparison of the change in Quasi-Biennial Oscillation amplitude at 70 hPa with the globally averaged surface temperature change in each of the aerosol only and greenhouse gas only experiments for the four models. The red best fit line is computed for the greenhouse gas only experiments and is constrained to go through the origin; this best-fit line is found to successfully predict the response to aerosols as well. The slope and uncertainty of a best-fit line using all experiments is included, and is statistically indistinguishable from that using just one of the two experiments.

et al., 2020c), and hence the lack of a robust change in period in the LESFMIP is expected. It would be interesting to revisit this result if CMIP6 models with stronger future change in period were to perform the LESFMIP experiments.

While our focus has been on changes robust across the four available models, there are differences among the four in the sensitivity to greenhouse gas and aerosol concentrations. HadGEM3 simulates the most pronounced response to aerosols, and also the strongest response of 50 hpa QBO winds to greenhouse gases. At 70 hPa, the strongest response is in IPSL, but HadGEM3 is next strongest (Figure 4). In contrast, MIROC6 and especially CNRM show weaker sensitivity to these external forcings (Figures 3 and 4). A potential explanation for this inter-model spread can be provided by the scaling analysis of Match and Fueglistaler (2021b), who show that surface warming and tropospheric expansion lead to an upward shift in the QBO by 6 hPa K^{-1}, with the scaling working best for the lower stratospheric part of the QBO. The amount of global warming in response to greenhouse gases and cooling in response to aerosols differs among these models (Figure S8 in Supporting Information S1), with HadGEM3 the most sensitive and MIROC6 the least sensitive. Figure 13 compares the change in the QBO at 70 hPa to the globally averaged temperature rise from the end to the beginning of the GHG-only and aerosol-only runs. A strong linear relationship exists between the two (correlation coefficient = −0.98), consistent with Match and Fueglistaler (2021b). A best-fit line computed for the GHG-only experiments successfully predicts the response to aerosols as well, and vice versa. This suggests that the mechanism underlying the changes in the QBO in response to greenhouse gases or aerosols is generic to either forcing. In contrast, changes in the QBO amplitude in response to volcanic eruptions cannot be explained by this framework —the QBO weakens even as the Earth's surface cools—and this weakening of the QBO arises via a separate dynamical process.

Future work is needed to understand both the seasonality and the sensitivity to QBO phase of disruption events, especially since it is plausible that disruption events will become more frequent in a world with higher GHG concentrations (Anstey et al., 2021). In addition, future work is needed to understand the role of these forcings for the surface response to the QBO, as in historical simulations with all forcings time varying the surface response is projected (paradoxically) to strengthen even as the QBO winds weaken (Rao et al., 2020c, 2023). Either way, the novel data set examined in this study allows for the attribution of historical changes of the QBO to different forcings, and highlights the crucial role played by greenhouse gases and volcanic eruptions.

Conflict of Interest

The authors declare no conflicts of interest relevant to this study.

Data Availability Statement

All data used in this study is available on the Earth System Grid Federation (ESGF; https://aims2.llnl.gov/search; Cinquini et al., 2014). This work used JASMIN, the UK's collaborative data analysis environment (https://www.jasmin.ac.uk; Lawrence et al., 2013).

Acknowledgments
DA and CIG acknowledge the support of the Israel Science Foundation (Grant agreement 1727/21). CIG is supported by the US-Israel Binational Science Foundation (BSF) Grant 2020316. SO would like to acknowledge support from the UK NERC NE/Y000048/1 and CANARI projects. We thank Aaron Match and an anonymous reviewer for their helpful comments.

References

Andrews, M. B., Ridley, J. K., Wood, R. A., Andrews, T., Blockley, E. W., Booth, B., et al. (2020). Historical simulations with HadGEM3-GC3. 1 for CMIP6. *Journal of Advances in Modeling Earth Systems*, *12*(6), e2019MS001995. https://doi.org/10.1029/2019ms001995

Anstey, J. A., Banyard, T. P., Butchart, N., Coy, L., Newman, P. A., Osprey, S., & Wright, C. J. (2021). Prospect of increased disruption to the QBO in a changing climate. *Geophysical Research Letters*, *48*(15), e2021GL093058. https://doi.org/10.1029/2021gl093058

Anstey, J. A., Osprey, S. M., Alexander, J., Baldwin, M. P., Butchart, N., Gray, L., et al. (2022). Impacts, processes and projections of the quasi-biennial oscillation. *Nature Reviews Earth & Environment*, *3*(9), 588–603. https://doi.org/10.1038/s43017-022-00323-7

Baldwin, M. P., Gray, L. J., Dunkerton, T. J., Hamilton, K., Haynes, P. H., Randel, W. J., et al. (2001). The quasi-biennial oscillation. *Review of Geophysics*, *39*(2), 179–229. https://doi.org/10.1029/1999rg000073

Boucher, O., Servonnat, J., Albright, A. L., Aumont, O., Balkanski, Y., Bastrikov, V., et al. (2020). Presentation and evaluation of the IPSL-CM6A-LR climate model. *Journal of Advances in Modeling Earth Systems*, *12*(7), e2019MS002010. https://doi.org/10.1029/2019ms002010

Brenna, H., Kutterolf, S., Mills, M. J., Niemeier, U., Timmreck, C., & Krüger, K. (2021). Decadal disruption of the QBO by tropical volcanic supereruptions. *Geophysical Research Letters*, *48*(5), e2020GL089687. https://doi.org/10.1029/2020gl089687

Brown, F., Marshall, L., Haynes, P. H., Garcia, R. R., Birner, T., & Schmidt, A. (2023). On the magnitude and sensitivity of the quasi-biennial oscillation response to a tropical volcanic eruption. *Atmospheric Chemistry and Physics*, *23*(9), 5335–5353. https://doi.org/10.5194/acp-23-5335-2023

Bushell, A., Anstey, J., Butchart, N., Kawatani, Y., Osprey, S., Richter, J., et al. (2022). Evaluation of the quasi-biennial oscillation in global climate models for the SPARC QBO-initiative. *Quarterly Journal of the Royal Meteorological Society*, *148*(744), 1459–1489. https://doi.org/10.1002/qj.3765

Butchart, N., Andrews, M. B., & Jones, C. D. (2023). QBO phase synchronization in CMIP6 historical simulations attributed to ozone forcing. *Geophysical Research Letters*, *50*(15), e2023GL104401. https://doi.org/10.1029/2023gl104401

Butchart, N., Anstey, J. A., Kawatani, Y., Osprey, S. M., Richter, J. H., & Wu, T. (2020). QBO changes in CMIP6 climate projections. *Geophysical Research Letters*, *47*(7), e2019GL086903. https://doi.org/10.1029/2019gl086903

Checa-Garcia, R. (2018). CMIP6 Ozone forcing dataset: Supporting information. *Zenodo*. https://doi.org/10.5281/zenodo.1135127

Checa-Garcia, R., Hegglin, M. I., Kinnison, D., Plummer, D. A., & Shine, K. P. (2018). Historical tropospheric and stratospheric ozone radiative forcing using the CMIP6 database. *Geophysical Research Letters*, *45*(7), 3264–3273. https://doi.org/10.1002/2017gl076770

Chiodo, G., Marsh, D., Garcia-Herrera, R., Calvo, N., & García, J. (2014). On the detection of the solar signal in the tropical stratosphere. *Atmospheric Chemistry and Physics*, *14*(11), 5251–5269. https://doi.org/10.5194/acp-14-5251-2014

Cinquini, L., Crichton, D., Mattmann, C., Harney, J., Shipman, G., Wang, F., et al. (2014). The earth system grid federation: An open infrastructure for access to distributed geospatial data [Dataset]. *Future Generation Computer Systems*, *36*, 400–417. https://doi.org/10.1016/j.future.2013.07.002

DallaSanta, K., Orbe, C., Rind, D., Nazarenko, L., & Jonas, J. (2021). Response of the quasi-biennial oscillation to historical volcanic eruptions. *Geophysical Research Letters*, *48*(20), e2021GL095412. https://doi.org/10.1029/2021gl095412

Findell, K. L., Sutton, R., Caltabiano, N., Brookshaw, A., Heimbach, P., Kimoto, M., et al. (2023). Explaining and predicting earth system change: A world climate research programme call to action. *Bulletin of the American Meteorological Society*, *104*(1), E325–E339. https://doi.org/10.1175/bams-d-21-0280.1

Fischer, P., & Tung, K. K. (2008). A reexamination of the QBO period modulation by the solar cycle. *Journal of Geophysical Research*, *113*(D7), D07114. https://doi.org/10.1029/2007JD008983

Garfinkel, C. I., Shaw, T. A., Hartmann, D. L., & Waugh, D. W. (2012). Does the Holton-Tan mechanism explain how the quasi-biennial oscillation modulates the arctic polar vortex? *Journal of the Atmospheric Sciences*, *69*(5), 1713–1733. https://doi.org/10.1175/JAS-D-11-0209.1

Gerber, E. P., & Manzini, E. (2016). The Dynamics and Variability Model Intercomparison Project (DynVarMIP) for CMIP6: Assessing the stratosphere–troposphere system. *Geoscientific Model Development*, *9*(9), 3413–3425. https://doi.org/10.5194/gmd-9-3413-2016

Givon, Y., Garfinkel, C. I., & White, I. (2021). Transient extratropical response to solar ultraviolet radiation in the Northern Hemisphere winter. *Journal of Climate*, *34*(9), 3367–3383. https://doi.org/10.1175/jcli-d-20-0655.1

Gray, L. J., Anstey, J. A., Kawatani, Y., Lu, H., Osprey, S., & Schenzinger, V. (2018). Surface impacts of the quasi biennial oscillation. *Atmospheric Chemistry and Physics*, *18*(11), 8227–8247. https://doi.org/10.5194/acp-18-8227-2018

Holton, J. R., & Tan, H. C. (1980). The influence of the equatorial Quasi-biennial Oscillation on the global circulation at 50 mb. *Journal of the Atmospheric Sciences*, *37*(10), 2200–2208. https://doi.org/10.1175/1520-0469(1980)037<2200:tioteq>2.0.co;2

Kang, M.-J., Chun, H.-Y., Son, S.-W., Garcia, R. R., An, S.-I., & Park, S.-H. (2022). Role of tropical lower stratosphere winds in quasi-biennial oscillation disruptions. *Science Advances*, *8*(27), eabm7229. https://doi.org/10.1126/sciadv.abm7229

Kawatani, Y., & Hamilton, K. (2013). Weakened stratospheric quasibiennial oscillation driven by increased tropical mean upwelling. *Nature*, *497*(7450), 478–481. https://doi.org/10.1038/nature12140

Kuai, L., Shia, R.-L., Jiang, X., Tung, K. K., & Yung, Y. L. (2009). Modulation of the period of the quasi-biennial oscillation by the solar cycle. *Journal of the Atmospheric Sciences*, *66*(8), 2418–2428. https://doi.org/10.1175/2009JAS2958.1

Kuchar, A., Ball, W. T., Rozanov, E. V., Stenke, A., Revell, L., Miksovsky, J., et al. (2017). On the aliasing of the solar cycle in the lower stratospheric tropical temperature. *Journal of Geophysical Research: Atmospheres*, *122*(17), 9076–9093. https://doi.org/10.1002/2017jd026948

Lawrence, B. N., Bennett, V. L., Churchill, J., Juckes, M., Kershaw, P., Pascoe, S., & Stephens, A. (2013). Storing and manipulating environmental big data with JASMIN [Software]. *In 2013 IEEE international conference on big data*, 68–75. Retrieved from https://www.jasmin.ac.uk

Martin, Z., Son, S.-W., Butler, A., Hendon, H., Kim, H., Sobel, A., et al. (2021). The influence of the quasi-biennial oscillation on the Madden–Julian oscillation. *Nature Reviews Earth & Environment*, *2*(7), 477–489. https://doi.org/10.1038/s43017-021-00173-9

Match, A., & Fueglistaler, S. (2021a). Anomalous dynamics of QBO disruptions explained by 1D theory with external triggering. *Journal of the Atmospheric Sciences*, *78*(2), 373–383. https://doi.org/10.1175/jas-d-20-0172.1

Match, A., & Fueglistaler, S. (2021b). Large internal variability dominates over global warming signal in observed lower stratospheric QBO amplitude. *Journal of Climate*, *34*(24), 9823–9836.

Ming, A., Hitchcock, P., & Haynes, P. (2016). The response of the lower stratosphere to zonally symmetric thermal and mechanical forcing. *Journal of the Atmospheric Sciences*, *73*(5), 1903–1922. https://doi.org/10.1175/JAS-D-15-0294.1

Oberländer-Hayn, S., Gerber, E. P., Abalichin, J., Akiyoshi, H., Kerschbaumer, A., Kubin, A., et al. (2016). Is the Brewer-Dobson circulation increasing or moving upward? *Geophysical Research Letters*, *43*(4), 1772–1779. https://doi.org/10.1002/2015gl067545

Osprey, S. M., Butchart, N., Knight, J. R., Scaife, A. A., Hamilton, K., Anstey, J. A., et al. (2016). An unexpected disruption of the atmospheric quasi-biennial oscillation. *Science*, *353*(6306), 1424–1427. https://doi.org/10.1126/science.aah4156

Rao, J., Garfinkel, C. I., Ren, R., Wu, T., Lu, Y., & Chu, M. (2023). Projected strengthening impact of the Quasi-Biennial Oscillation on the Southern Hemisphere by CMIP5/6 models. *Journal of Climate*, *36*(16), 5461–5476. https://doi.org/10.1175/jcli-d-22-0801.1

Rao, J., Garfinkel, C. I., & White, I. P. (2020a). How does the quasi-biennial oscillation affect the boreal winter tropospheric circulation in CMIP5/6 models? *Journal of Climate*, *33*(20), 8975–8996. https://doi.org/10.1175/JCLI-D-20-0024.1

Rao, J., Garfinkel, C. I., & White, I. P. (2020b). Impact of the quasi-biennial oscillation on the northern winter stratospheric polar vortex in CMIP5/6 models. *Journal of Climate*, *33*(11), 4787–4813. https://doi.org/10.1175/JCLI-D-19-0663.1

Rao, J., Garfinkel, C. I., & White, I. P. (2020c). Projected strengthening of the extratropical surface impacts of the stratospheric quasi-biennial oscillation. *Geophysical Research Letters*, *47*(20), e2020GL089149. https://doi.org/10.1029/2020gl089149

Richter, J. H., Butchart, N., Kawatani, Y., Bushell, A. C., Holt, L., Serva, F., et al. (2022). Response of the quasi-biennial oscillation to a warming climate in global climate models. *Quarterly Journal of the Royal Meteorological Society*, *148*(744), 1490–1518. https://doi.org/10.1002/qj.3749

Santer, B. D., Wehner, M. F., Wigley, T., Sausen, R., Meehl, G., Taylor, K., et al. (2003). Contributions of anthropogenic and natural forcing to recent tropopause height changes. *Science*, *301*(5632), 479–483. https://doi.org/10.1126/science.1084123

Shibata, K. (2021). Simulations of ozone feedback effects on the equatorial quasi-biennial oscillation with a chemistry–climate model. *Climate*, *9*(8), 123. https://doi.org/10.3390/cli9080123

Shiogama, H., Tatebe, H., Hayashi, M., Abe, M., Arai, M., Koyama, H., et al. (2023). MIROC6 Large Ensemble (Miroc6-Le): Experimental design and initial analyses. *Earth System Dynamics Discussions*, *2023*(6), 1–28. https://doi.org/10.5194/esd-14-1107-2023

Smith, D. M., Gillett, N. P., Simpson, I. R., Athanasiadis, P. J., Baehr, J., Bethke, I., et al. (2022). Attribution of multi-annual to decadal changes in the climate system: The Large Ensemble Single Forcing Model Intercomparison Project (LESFMIP). *Frontiers in Climate*, *4*, 955414. https://doi.org/10.3389/fclim.2022.955414

Tatebe, H., Ogura, T., Nitta, T., Komuro, Y., Ogochi, K., Takemura, T., et al. (2019). Description and basic evaluation of simulated mean state, internal variability, and climate sensitivity in MIROC6. *Geoscientific Model Development*, *12*(7), 2727–2765. https://doi.org/10.5194/gmd-12-2727-2019

Voldoire, A., Saint-Martin, D., Sénési, S., Decharme, B., Alias, A., Chevallier, M., et al. (2019). Evaluation of CMIP6 deck experiments with CNRM-CM6-1. *Journal of Advances in Modeling Earth Systems*, *11*(7), 2177–2213. https://doi.org/10.1029/2019MS001683

Wallace, J. M., Panetta, R. L., & Estberg, J. (1993). Representation of the equatorial stratospheric quasi-biennial oscillation in EOF phase space. *Journal of the Atmospheric Sciences*, *50*(12), 1751–1762. https://doi.org/10.1175/1520-0469(1993)050<1751:rotesq>2.0.co;2

Wang, Y., Rao, J., Lu, Y., Ju, Z., Yang, J., & Luo, J. (2023). A revisit and comparison of the quasi-biennial oscillation (QBO) disruption events in 2015/16 and 2019/20. *Atmospheric Research*, *294*, 106970. https://doi.org/10.1016/j.atmosres.2023.106970

Watanabe, S., & Kawatani, Y. (2012). Sensitivity of the QBO to mean tropical upwelling under a changing climate simulated with an earth system model. *Journal of the Meteorological Society of Japanese Series II*, *90*, 351–360. https://doi.org/10.2151/jmsj.2012-a20